Marine Geophysical Researches **23:** 299–318, 2002.

Study of the Saldanha Massif (MAR, 36°34′ N): Constrains from rock magnetic and geophysical data

J. M. Miranda[1], P. F. Silva[1,2], N. Lourenço[3], B. Henry[4], R. Costa[5] & the Saldanha Team[6]
[1]*Centro de Geofísica da Universidade de Lisboa, Portugal,* [2]*Instituto Superior de Engenharia de Lisboa, Portugal,* [3]*Centro de Investigação Marinha e Ambiental da Universidade do Algarve, Portugal,* [4]*Institut de Physique du Globe de Paris and CNRS, France,* [5]*CREMINER-FCUL, Portugal,* [6]*Saldanha Team (A. Almeida, F. J. Barriga, M. Biscoito, J. L. Charlou, A. Dias, Y. Fouquet, A. Marques, F. Porteiro, G. Queiroz, K. Olu, L. M.Victor)*

Received 22 May 2002; accepted 28 March 2003

Key words: detachment fault, NTO tectonics, rock magnetism

Abstract

We present a study of the magnetic properties of a group of basalt samples from the Saldanha Massif (Mid-Atlantic Ridge – MAR – 36° 33′ 54″ N, 33° 26′ W), and we set out to interpret these properties in the tectono-magmatic framework of this sector of the MAR. Most samples have low magnetic anisotropy and magnetic minerals of single domain grain size, typical of rapid cooling. The thermomagnetic study mostly shows two different susceptibility peaks. The high temperature peak is related to mineralogical alteration due to heating. The low temperature peak shows a distinction between three different stages of low temperature oxidation: the presence of titanomagnetite, titanomagnetite and titanomaghemite, and exclusively of titanomaghemite. Based on established empirical relationships between Curie temperature and degree of oxidation, the latter is tentatively deduced for all samples. Finally, swath bathymetry and sidescan sonar data combined with dive observations show that the Saldanha Massif is located over an exposed section of upper mantle rocks interpreted to be the result of detachment tectonics. Basalt samples inside the detachment zone often have higher than expected oxidation rates; this effect can be explained by the higher permeability caused by the detachment fault activity.

Introduction

The Mid-Atlantic Ridge (MAR) south of the Azores Triple Junction has been extensively studied in recent years through the FARA (French American Ridge Atlantic) program, and by several international research programs focused on hydrothermal research, including MARFLUX/ATJ (Bougault et al., 1996, 1998) and AMORES (Fouquet et al., 1997). The non-transform offset (NTO) between the AMAR and FAMOUS segments (see Figure 1 for location) was mapped during the FARA-SIGMA cruise in 1991 by EM12 swath bathymetry (Needham et al., 1992), and hydrothermal activity in the water column was first detected during the FAZAR cruise in 1992 (Langmuir et al., 1993; Klinkhammer et al., 1992, Charlou et al., 1993). These data were later confirmed by dynamic hydrocasts during the HEAT cruise (German et al. 1996; Bougault et al., 1998).

The FLAME cruise (German et al., 1998) continued geochemical exploration and three dives with the NAUTILE submersible were made along the floor of the NTO during the FLORES cruise (Fouquet et al., 1997). These dives failed to detect a discrete hydrothermal plume source, but provided the first geological exploration of the seafloor and confirmed that CH_4 anomalies were derived from upper mantle rocks.

In 1998, the SALDANHA cruise on N/O Nadir (Barriga et al., 1999), conducted a series of five NAUTILE dives on the eastern sector of the FAMOUS-AMAR NTO over a dome structure, thereafter designated as the Saldanha Massif. This cruise enabled geological exploration and confirmation that the seafloor in the dome and its vicinity is composed of serpentinites. Additionally, the expedition identified a small area 50 × 50 m wide, where weak, diffuse discharges of clear, gas-bearing fluid were observed. During the submersible exploration, seafloor rocks were systematically sampled, and relevant tectonic and structural information was acquired.

In this work we present a study of 30 basalt blocks (see Figure 2 for sample locations) collected on dives from the FLORES and SALDANHA cruises, and we use their magnetic properties to character-

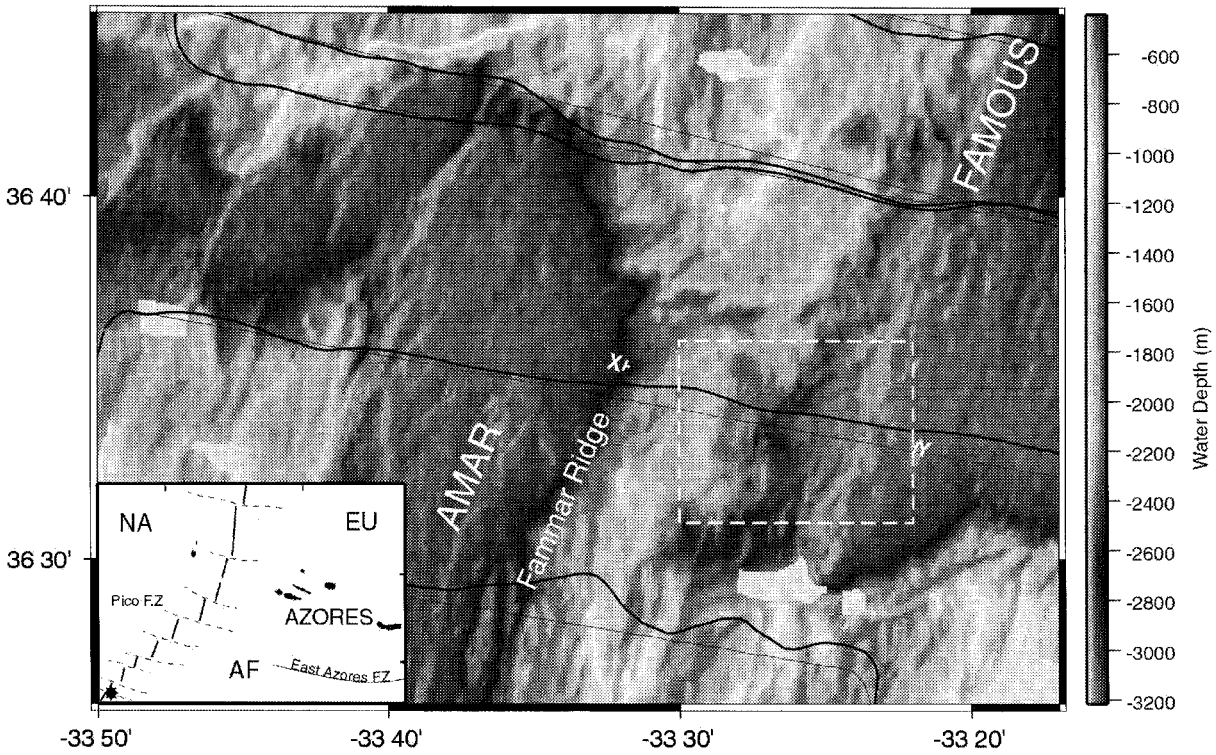

Figure 1. Shaded bathymetric map of the FAMOUS-AMAR non-transform offset. Illumination from the west. Dashed white box corresponds to the area shown in Figures 3 and 4, where a 20 × 20 m bathymetric grid was produced. Wiggles (thick black lines) are sea-surface anomalies plotted along ship tracks (thin black lines) resulting from the merging of SudAzores (Cannat et al., 1999) and SIGMA cruise (Needham et al., 1992), with positive anomalies to the north and negative to the south. Wiggle scale 2500nT/cm. X – Y, location of the topographic profile presented in Figure 14C). Inset: Location of the study area in the North Atlantic. Black star signals the FAMOUS-AMAR discontinuity. EU, NA and AF are respectively Eurasian, North-American and African plates.

ize the tectono-magmatic processes that affected the genesis of the Saldanha Massif. We discuss the implications of this data for the observed geological and morphostructural characteristics of the Saldanha Massif.

Cartographic sources of information used in this work consist of two E-W TOBI (Towed Ocean Bottom Instrument) tracks made during the HEAT cruise (German et al., 1996) that were used to produce 231 km^2 of imagery of the study area, with 6 m pixel size and 256 levels of backscatter. Another source of morphological information comes from the high-resolution bathymetric survey made during the FLORES cruise (Fouquet et al., 1997). This survey allowed the computation of a 20 m resolution bathymetric grid, which was coupled with the TOBI data to provide a more detailed picture of the Saldanha's morphology and geology. Outside this area a lower resolution bathymetric grid (100 × 100 m) was used, obtained from the SIGMA (Needham et al., 1992) and SUD-AZORES (Cannat et al., 1999) cruises. Seafloor geology observations were retrieved from three dives from the FLORES cruise and all of the dives from the SALDANHA cruise in the area.

Geological Setting

The study area lies within a second order NTO zone that separates the AMAR spreading segment to the south from the FAMOUS segment to the north. The NTO is characterized by a series of cross-cutting discontinuous faults that define an oblique en-echelon pattern. The fault systems within the NTO strike E-W, NNW-SSE and E-W (Gracia et al., 2000; Parson et al., 2000). In the non-transform area, two main structures can be recognized: the first is a narrow feature, trending 025°, and defining the eastern flank of the AMAR segment, designated as FAMMAR ridge by Bougault et al. (1998). The second is the subject of this study, the Saldanha Massif. Ship-borne magnetic profiles (Figure 1), crossing the FAMMAR ridge, display consistently high positive amplitudes suggesting

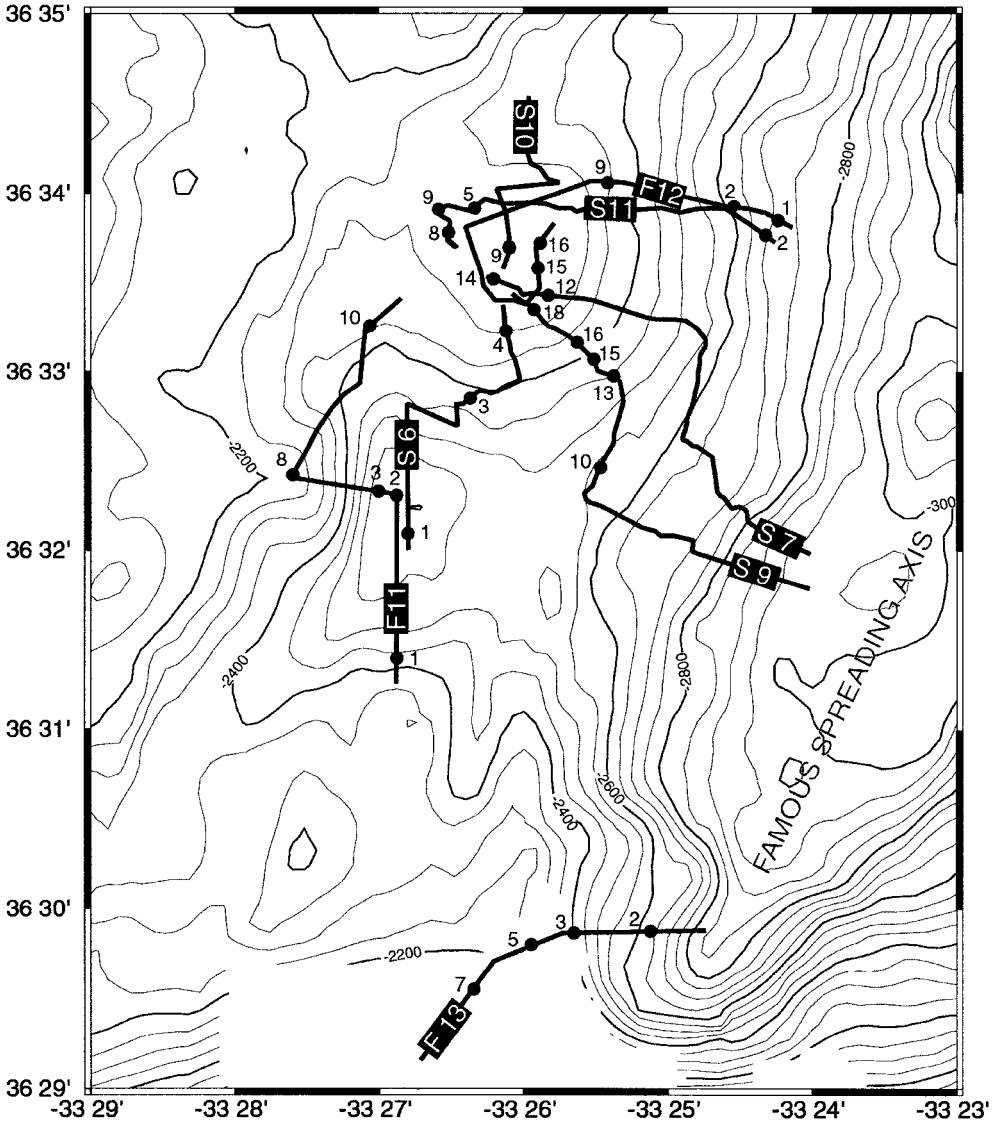

Figure 2. Saldanha Massif bathymetric map with sample and dive locations. Contour interval is 50 m.

a volcanic origin for this ridge. Over the Saldanha Massif, a clear decrease in amplitude is observed in the magnetic profile, which is attributed to cropping out of serpentinized mantle.

Bathymetric expression of the FAMOUS valley western wall is still traceable within the FAMOUS-AMAR NTO domain up to 36°30′ N parallel. Here it terminates against shallower AMAR-generated abyssal hill topography. In plan view the FAMOUS western wall displays a structure with NNE-SSW sections alternating with others oriented in a WNW-ESE direction which correspond to areas of depressed bathymetry. The Saldanha Massif is located north of one of these intersections (Figure 1).

The Saldanha Massif is a 100 m high (between −2300 m and −2200 m deep) semi-circular dome that is slightly elongated in the NNE-SSW direction. Its eastern flank extends towards the FAMOUS spreading segment to a water depth of −3200 m. The Massif itself lies in a 32 km^2 area of smooth topography, detached from the FAMOUS segment western wall, with slopes dipping from 010° to 020°. Detailed analysis of the dome structure from TOBI and high resolution bathymetric images (Figures 3, 4 and 14) reveal that this surface is disrupted by high angle normal faults strik-

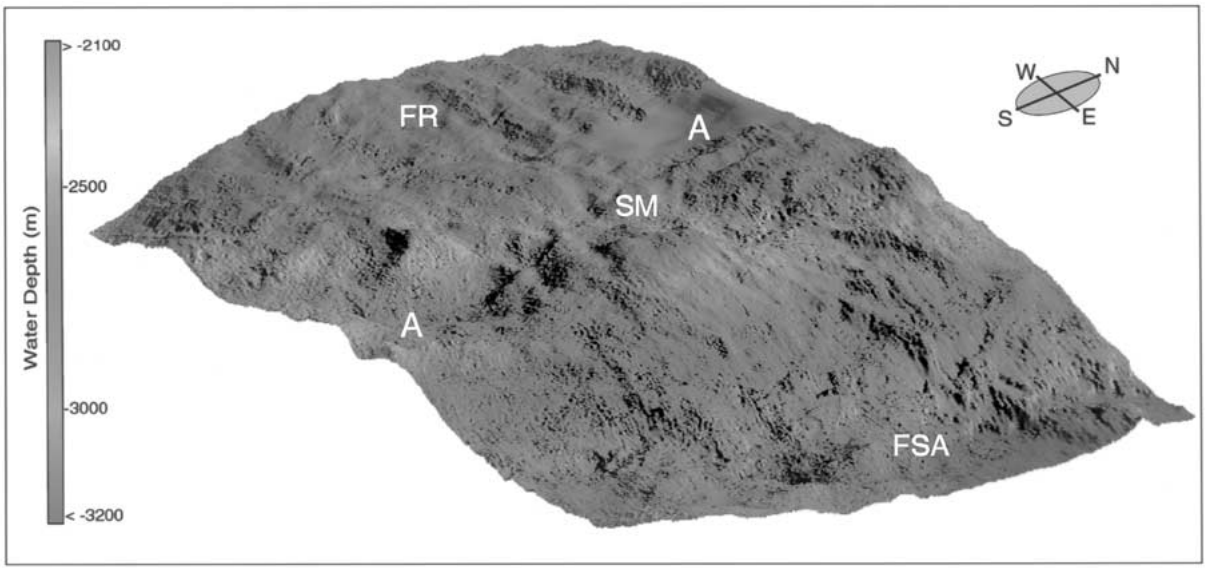

Figure 3. Perspective shaded relief plot of 20 × 20 m bathymetric grid. Sun azimuth 35°, sun angle 30°. View from SE. Vertical exaggeration 2x. FR – FAMMAR Ridge. SM – Saldanha Massif. FSA – FAMOUS Spreading Axis. A – Elongated NNW-SSE depression discussed in text.

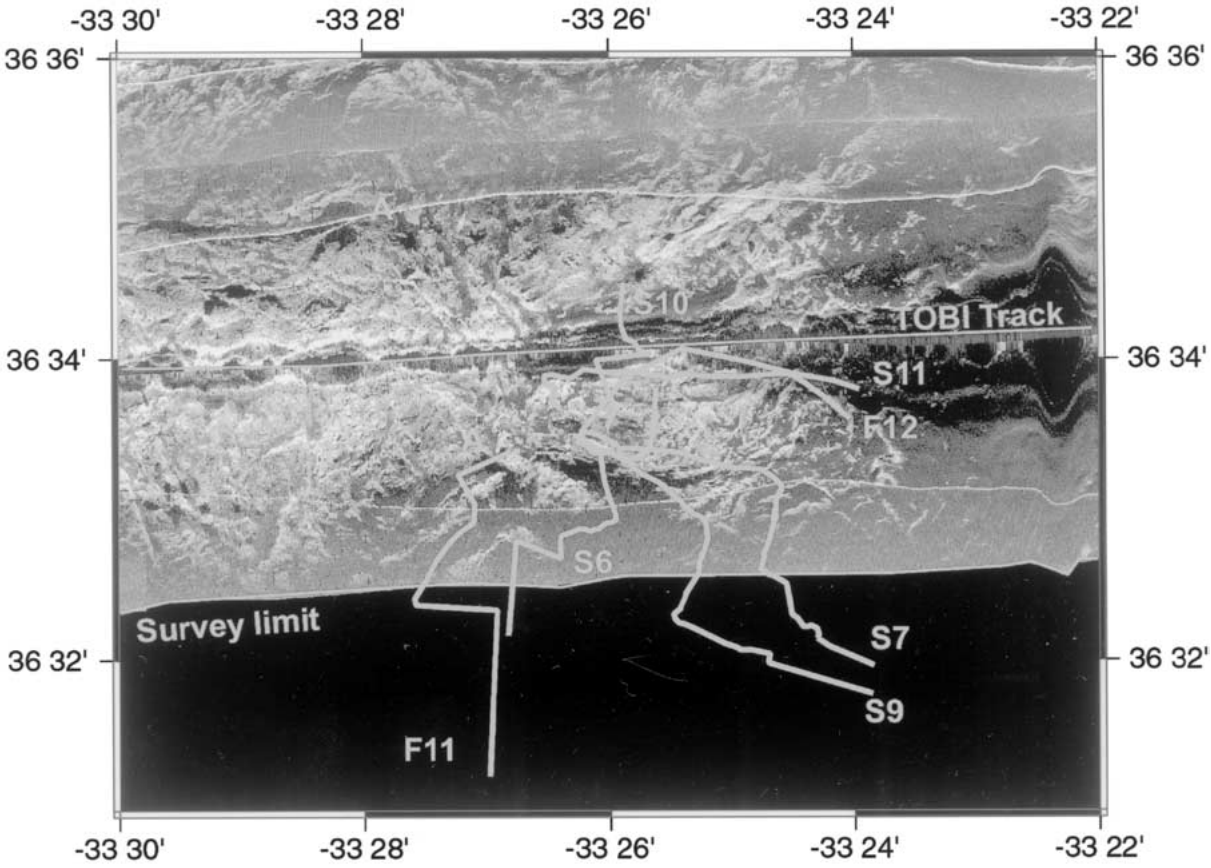

Figure 4. TOBI Sidescan sonar data. Dive tracks are also shown for reference. Note the acoustic signature of depression AA, and the WNW-ESE lineations on the top and eastern flank of the massif.

ing NE-SW, sub-parallel to the dome's major axis. The dome surface presents a series of low amplitude steps and ridges (Figures 3 and 4), striking approximately E-W to WNW-ESE. These structures are clearly defined on the dome, and become gradually less traceable towards the northern flank. Nevertheless they seem to be confined to the area where serpentinized mantle outcrops are documented from dive observations.

The geographical limits of this exposed mantle section can also be tentatively constrained from morpho-structural data. The western limit is delineated by a sharp NNW-SSE trending linear depression 70 to 150 m deep (AA in Figures 3, 4, and 14). This depression is interpreted in TOBI images from two aligned segments with a dull acoustic tone, probably due to a high degree of sedimentation. To the east, abundant serpentinite outcrops were observed from dives S7 and S9 at −2900 m water depth, and hence in the vicinity of the FAMOUS valley axis. In the FAMOUS valley floor adjacent to this domain, TOBI images show predominantly volcanic textures (hummocks, seamounts and flows), together with minor faulting and fissuring (Parson et al., 2000), suggesting that the transition between mantle outcrops and crust generated by seafloor spreading should be located around the −3100 m isobath. The northern limit of the Massif is unclear. It should probably be set at the intersection between the AA depression with a series of E-W elongated basins, showing a left-lateral en-echelon pattern at the base of the northern NTO edge (Figure 1). South of the Saldanha Massif, the limit should be located near the 36°32′ N parallel (Figure 15), at the tip of the AA depression. Here the relief steepens and a set of NNE-SSW faults is observed.

Geology from dives

Diving was used both to study the spatial distribution of lithologies and to describe the nature of the E-W lineations in the sonar images on the dome.

Despite the high reflectivity that can be observed on the TOBI imagery, submersible observations showed high degrees of sedimentation cover (generally between 80% and 100%), the only observed exceptions being the base of NE-SW high angle fault scarps, which are covered with fresh talus deposits suggesting a more recent genesis for these structures. Scattered exposures were composed not of *in situ* outcrops but rather of talus deposits of varying types. The succession of lithotypes observed during dives over the Saldanha Massif does not correspond to a typical layout of oceanic crust.

In Figure 5, we present three geological cross-sections from dives inside (S11 and S9) and outside (F11) the Massif. We generalize the observations over the Saldanha Massif flanks using two major units: serpentinite-dominated tectonic breccias and volcanic-dominated tectonic breccias. The latter are composed of volcanic breccias, pillow lavas and massive lava fragments. We should emphasize, however, that the definition of these units is mainly based on the analysis of samples retrieved from the seafloor and thus subject to biasing in the sampling process, because of the compositional heterogeneity of outcrops and the degree of pelagic sedimentation. Other lithologies can therefore be present but not sampled.

The upper surface of the Saldanha Massif was intensively covered by dives that found a highly heterogeneous tectonic mélange, with metagabbros, pillow fragments and volcanic breccias, serpentinites and talc-bearing serpentinites, affected heterogeneously by metasomatic processes, and indurated sediment.

The SE flank, surveyed during dives S7 and S9 (Figure 5), displays serpentinite breccias at the base of the slope (∼ −2900 m). At −2700 m a sharp transition to a series of highly brecciated, reworked and oxidized, basaltic blocks was documented on dive S9. About 600 m further upslope, serpentinites again become the dominant lithotype, frequently occurring in ridges along isobaths. In the sub-parallel S7 dive track at the same water depth interval only serpentinites were sampled. Between −2550 m and −2440 m water depth (Figure 5) basaltic dikes were observed in both dives S7 and S9. Their relation with underlying serpentinites is not clear and we are unable to distinguish them as upper crustal volcanic feeders. From 2440 m water depth to the top of the Massif at 2200 m water depth, the main lithologies are oxidized volcanic breccias, sometimes in scattered blocks, and minor fragmented pillow basalts.

Dive S11 (Figure 4) performed an E-W transect to the top of the Saldanha Massif. Unlike dives S7 and S9, the base of the dive, between −2700 m and −2400 m water depth, is composed of volcanic-dominated tectonic breccia. Outcrops of serpentinites are documented at higher levels, between −2300 m and the top of the Massif. Confirming the somewhat random occurrence of different lithologies, it should be pointed out that dive F12, following a track located very near dive S11, sampled metagabbros, whereas S11 did not yield any occurrence of this lithology.

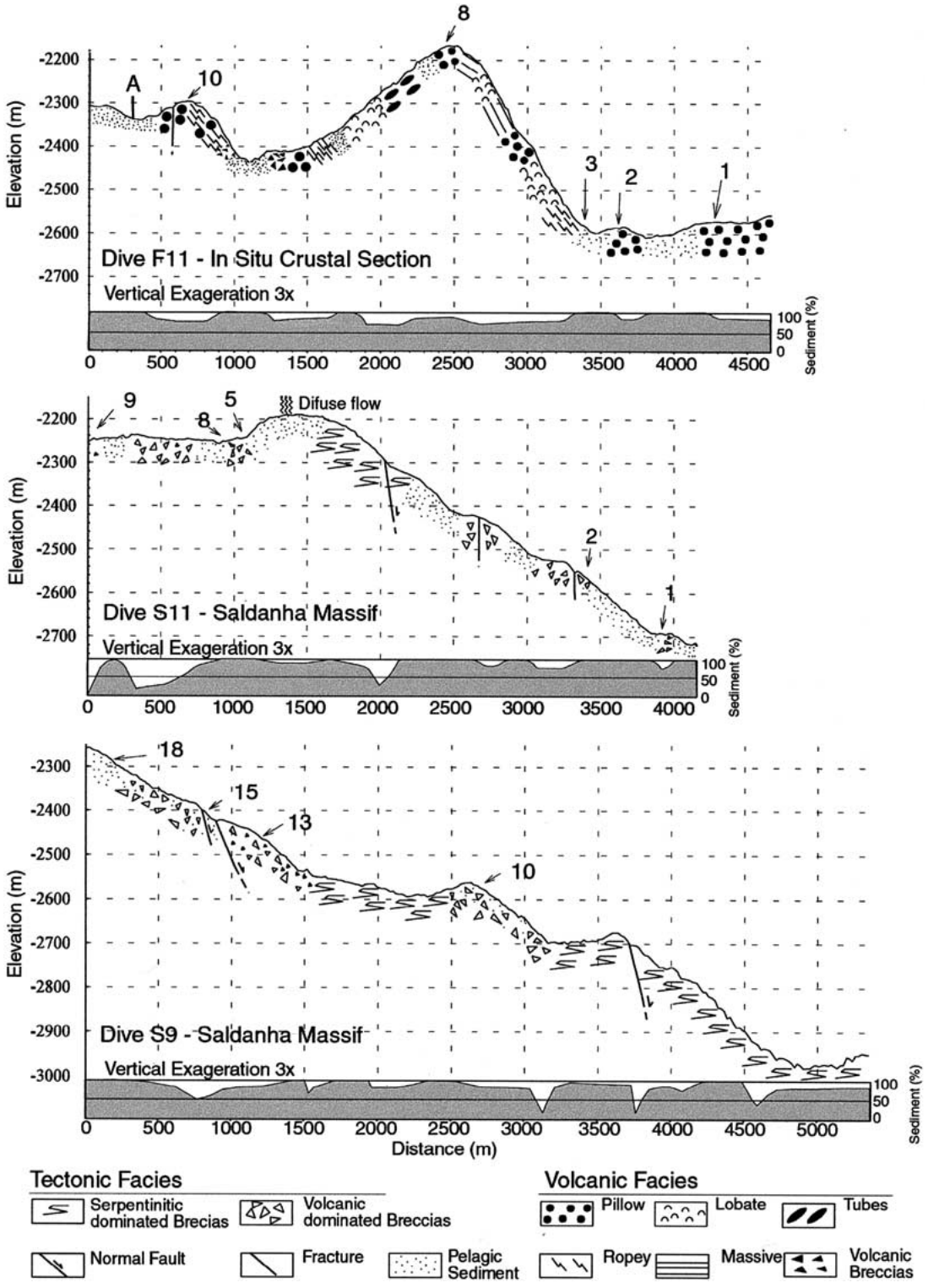

Figure 5. Schematic geologic cross sections obtained from representative dives with sample locations along each dive track.

Dive S10 provided a N-S transect from −2360 m water depth up to the top of the Massif. Despite almost 100% sediment cover during the dive all the rocks sampled in the first 600 m of the dive track are talc-bearing serpentinites, confirming the assessment that mantle rocks are not confined to the dome itself and crop out in a broader area.

To evaluate the structural significance of depression AA we used data provided by dives F11 (Figure 5) and S6. Dive F11 dive was performed west of depression AA. All the observed outcrops are volcanic in nature, and represent dominantly lava facies. Little tectonization is observed, and the style of outcropping suggests that these volcanic units are *in situ*. The end of dive F11 is made over depression AA, and confirms a high degree of sedimentation. Dive S6 displayed a drastic change in the seafloor geology prior and subsequent to depression AA. The beginning of dive S6 revealed geology similar to that seen during dive F11. However, as the dive track crossed depression AA, the outcropping style became dominated by the same heterogeneous volcanic and serpentinite-dominated tectonic breccias observed in the other dives over the Massif. These observations strongly suggest that depression AA is a significant tectonic boundary, which separates a crustal domain to the west from the serpentinized mantle outcrops of the Saldanha Massif to the east.

Finally, Dive F13 was used to study the southern limit of the Saldanha Massif. Dive F13 followed a path from the nodal deep at the end of the FAMOUS segment, westward over the valley wall into a series of NNE-SSW abyssal hills associated with the AMAR segment. This dive documented *in-situ* volcanic material that was less sedimented, and no ultramafics were reported.

Anisotropy of Magnetic Susceptibility (AMS) Study

From the SALDANHA and FLORES dives we were able to recover a group of 30 basalt blocks from the Saldanha Massif and surrounding area, obtaining a total of 60 drilled cylindrical samples (2.5 cm in diameter by 2.1 cm high), which were used for rock-magnetism studies.

Most samples have bulk susceptibilities ranging from 2×10^{-3} to 10×10^{-3} SI. A single group of analyses, from sample S9-13, displays slightly higher values, ranging from 10×10^{-3} to 20×10^{-3} SI (Figure 6). Jelinek's (1981) diagram for all basalt samples (Figure 7) shows that the values of P' (corrected degree of anisotropy) are very low, less than 1.015, and that the susceptibility ellipsoid has no preferential shape. The only exception once again is found in sample S9-13, where P' reaches 1.03–1.045 with a well-defined oblate shape of the susceptibility ellipsoid.

The magnetic fabric was studied for all recovered basalts of sufficient size to allow drilling of standard samples in the laboratory. Samples were oriented with respect to an imaginary axis, fixed to each sample, and their AMS measured with a KLY-2 Kappabridge.

Only oriented samples from sample S9-13 showed significant magnetic fabric, with the maximum and intermediate axes distributed along a great circle, and very well clustered minimum axis (Figure 8). No other samples show any coherent magnetic fabric.

To determine whether the lack of coherent magnetic fabric is the consequence of measurement uncertainty or actual incoherence, in Figure 9 we present the size of the 95% confidence interval for the principal axes of all samples (Jelinek, 1977). Samples with P' values lower than 1.015 exhibit large confidence intervals, particularly for the lowest anisotropies, while S9-13 samples have low measurement uncertainty values. However, for at least some of the samples, the measurement uncertainty appears insufficient to explain the lack of a coherent magnetic fabric. In contrast to lava flows, which mostly show relatively regular magnetic fabric (see for example Canon-Tapia et al., 1995), Saldanha Massif basalts have no coherent AMS, probably indicating fast cooling without well organized flowing.

Magnetic Mineralogy

The compositional variability of magnetic minerals included in basalts depends mainly on magma composition, magmatic gas composition, cooling rate and subsequent chemical interactions with the environment, in particular the effects of seawater circulation. The main magnetic carrier for submarine basalts is usually the Fe-Ti oxide titanomagnetite. The chemical equation of titanomagnetites can be represented as $Fe_{3-x}Ti_xO_4$, where x is a parameter varying between 0 and 1, characterizing the molar proportion of Ti^{4+} ($x = 1$ corresponds to ulvospinel and $x = 0$ to magnetite). Recent work (e.g., Xu et al., 1997a, b; Zhou et al., 1997, 2000, 2001) has used high-resolution electron microscopy to identify the composition and

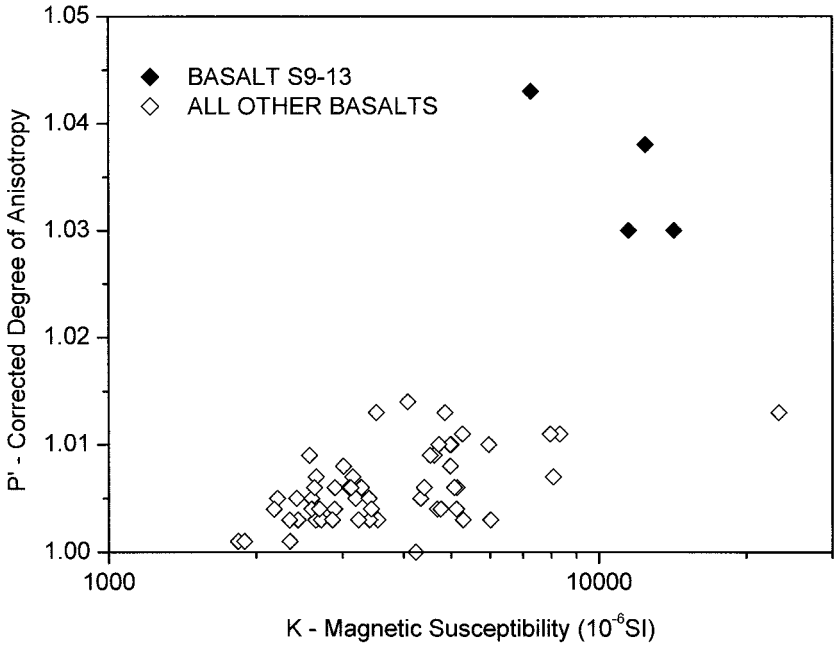

Figure 6. Magnetic susceptibility K versus corrected degree of anisotropy P′ $P' = \exp\sqrt{2[(n_1 - n_m)^2 + (n_2 - n_m)^2 + (n_3 - n_m)^2]}$, where $n_i = \ln K_i$, K_i being the principal susceptibility values $K_1 \geq K_2 \geq K_3$ and K_m the geometric mean of the principal susceptibility values). The five samples that display higher values of susceptibility and anisotropy belong to sample S-09-13.

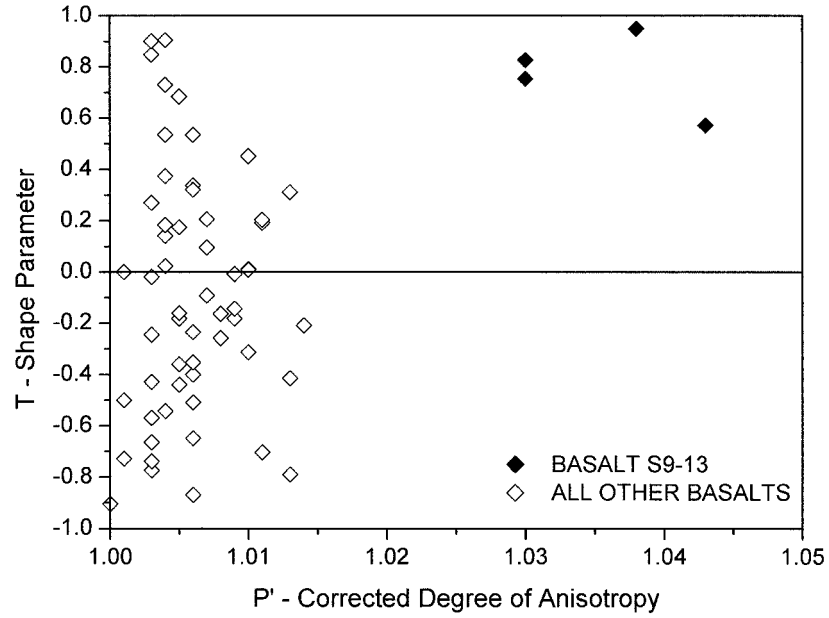

Figure 7. Jelinek's (1981) diagram: Corrected Degree of Anisotropy (P′) versus Shape Parameter ($T = [2(n_2 - n_3)/(n_1 - n_2)] - 1$).

magnetic mineralogy and to better understand oxidation effects in oceanic basalts. Zhou et al. (2000) classified two distinct groups from the point of view of magnetic mineralogy. The first group is characterized by larger grains, displaying an average composition $x = 0.6$ within a narrow range (x between 0.55 and 0.69) and corresponds to the interior of pillow lavas (i.e., > 3 cm from the pillow rim); these results are similar to those already determined by Irving (1970), Johnson and Hall (1978), Peterson et al. (1979) and

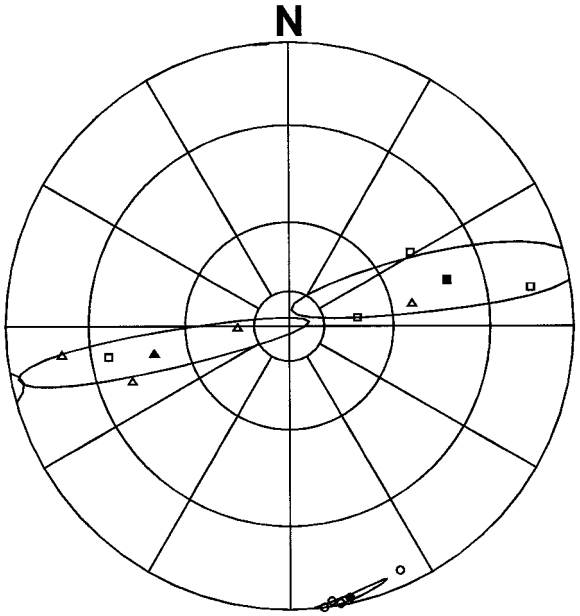

Figure 8. Stereographic projection in the lower hemisphere displaying the magnetic fabric of the S9-13 basalt sample: maximum (square), intermediate (triangle) and minimum (circle) susceptibility axes for each sample (open symbols) and for the mean tensor (filled symbols) with the associated 95% confidence intervals. N indicates an imaginary North for the sample.

Smith-Daignières (1984). The second group is characterized by tiny grains embedded within quenched interstitial glass, with a compositional variation that ranges across almost all the solid solution spectrum, with an average molar Ti^{4+} value of $x = 0.45$.

Titanomagnetites from oceanic basalts undergo to a low-temperature oxidation process known as maghemitization. This process is characterized by the diffusion of Fe^{2+} ions to the surface of the crystal, resulting in the cation-deficient spinel titanomaghemite (Dunlop and Ozdemir, 1997): $Fe^{3+}_{(2+2z/3)}Fe^{2+}_{(1-z)\square(z/3)}O^{2-}_4$, where z is the oxidation parameter varying between 0 and 1, and $\square$ indicates a lattice vacancy. The processes associated with oceanic basalt oxidation are very complex and can develop on different scales, mainly related to the permeability of the oceanic crust on the regional or local scale, porosity of the rocks (Alt et al., 1986; Honnorez et al., 1996), and oxygen fugacity and granularity (Gallagher et al., 1968). The rate at which oxidation develops is different for the two groups of magnetic minerals already mentioned. While large grains tend to oxidize gradually with age, tiny grains tend to preserve their original properties as long as the interstitial glass remains (Zhou et al., 1999).

Magnetic grain size distribution

The grain size distribution of magnetic minerals was studied in 30 samples of basalts with hysteresis loop measurements, using a translation inductometer within an electromagnet. The analysis of hysteresis parameters (Day et al., 1977; Dunlop, 1986a, 1986b) reveals predominantly single domain grain size (SD in Figure 10), typical of basalts with rapid cooling, emplaced in oceanic conditions. The only exception to this result is found for sample S9-13, which is characterized by higher coercive ratio values (H_{cr}/H_c), corresponding to pseudo-single domain grain size (PSD in Figure 10).

Thermomagnetic curves

Peaks of susceptibility on thermomagnetic curves (magnetic susceptibility in low field K as a function of temperature) can be related to the Hopkinson effect (due to superparamagnetic behavior of magnetic grains close to the Curie point) or to mineralogical alteration. A similarly steep decrease of susceptibility indicates Curie temperature as well as mineralogical alteration. The occurrence of mineralogical alteration is shown by the difference between heating and cooling curves. Curie temperatures (T_c) are determined from the inflection point of the curve (Chevallier and Pierre, 1932). Thermomagnetic curves for 30 basalt samples were studied in an argon controlled atmosphere, up to a maximum temperature of 700 °C. Partial curves with lower maximum temperature were made in order to reveal possible mineralogical alterations by irreversible curves.

Complex shapes characterize the thermomagnetic cycles from the Saldanha samples (Figure 11), suggesting the presence of several magnetic phases. Partial loops reveal that none of the curves are reversible after heating to 300 to 400 °C, indicating mineralogical alterations. The second susceptibility peak that occurs during heating at higher temperatures corresponds to the formation of new minerals with higher magnetic susceptibility. This behavior is interpreted as the result of titanomaghemite (original magnetic phase) instability caused by heating, with inversion to a multiphase intergrowth, such as magnetite, ilmenite and other minerals (Readman and O'Reilly, 1972; Ozdemir, 1987). In the following discussion, only the temperature window corresponding to the reversible portion of the curve will be considered.

Based on the shape of the thermomagnetic curves, the cycles have been separated into three main groups

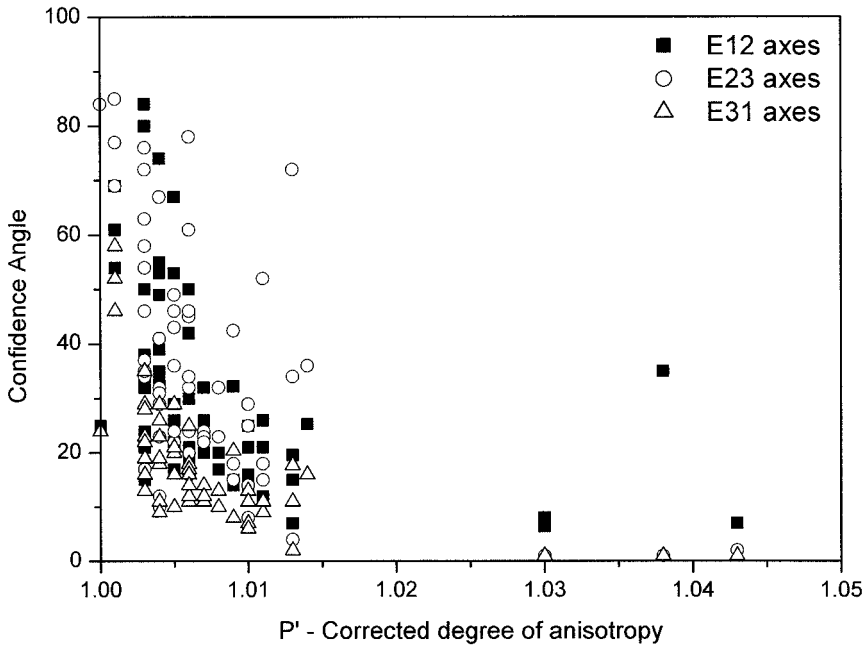

Figure 9. For each sample, corrected degree of anisotropy P′ versus α_{95} confidence angles for each principal axis of the susceptibility ellipsoid in the plane including K_1 and K_2 axes (E12), K_2 and K_3 axes (E23), and K_3 and K_1 axes (E31).

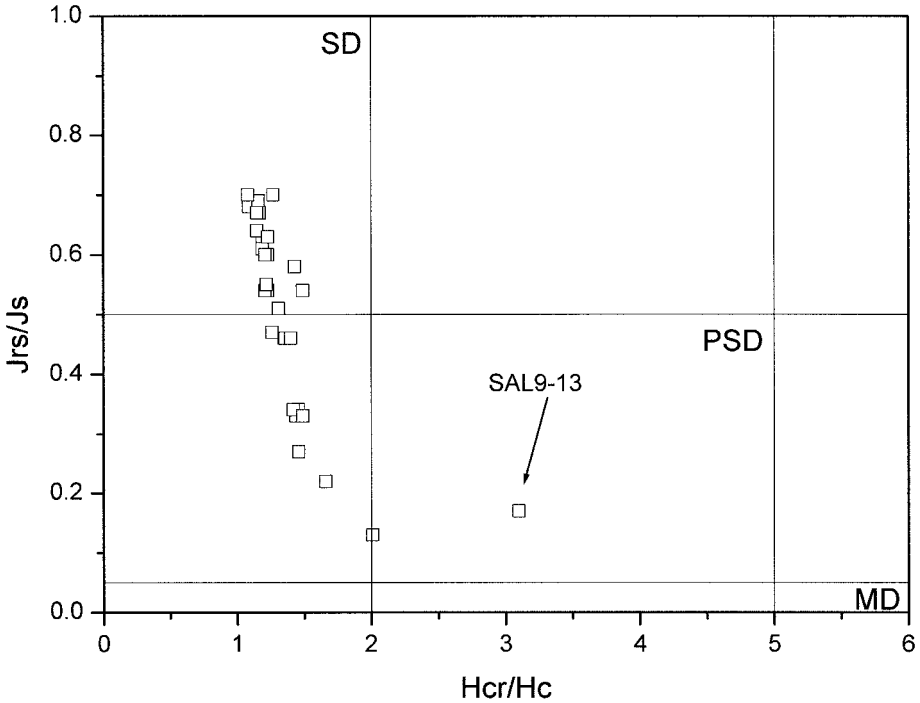

Figure 10. Day et al. (1977) plot of saturation magnetization ratio (Jrs/Js) versus coercive force ratio (Hcr/Hc) for the basalt samples. Regions of Jrs/Js – Hcr/Hc space where single domain (SD), pseudo-single domain (PSD) and multi-domain (MD) grain sizes predominate are indicated.

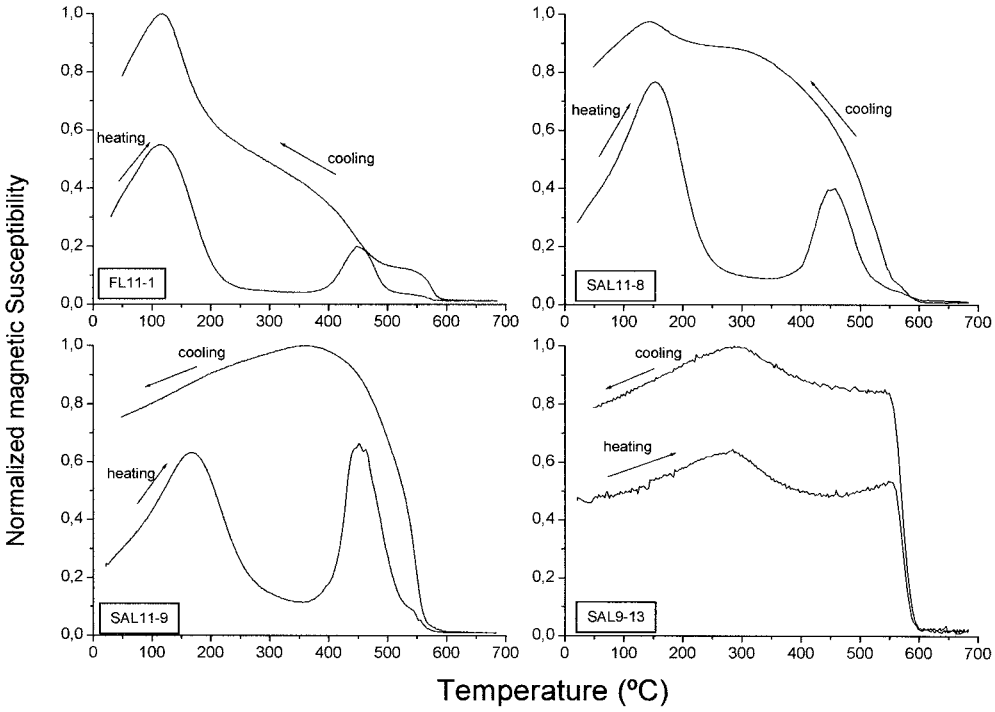

Figure 11. Examples of typical thermomagnetic curves of the Saldanha Massif basalt samples. The arrows indicate the sense of the thermomagnetic cycle. The experiments were performed in an argon-controlled atmosphere.

(Table 1). Group I corresponds to those samples that preserve their original magnetic phase after heating (Figure 11; e.g., sample F11-1). In this case, the same Hopkinson effect was observed on the heating and cooling curves, but there are also mineralogical alterations at high temperature. Unlike titanomagnetite, titanomaghemite should alter to other minerals for temperatures much lower than 600 °C. Because 700 °C was the maximum temperature reached before cooling started, the presence of a Hopkinson effect during cooling is interpreted as being related to the original titanomagnetite.

Group II is characterized by the presence of two magnetic phases, which we interpret as titanomagnetite and titanomaghemite. In this case, a Hopkinson effect was observed on both the heating and the cooling curves, but with a different shape and sometimes corresponding to slightly different temperatures (Figure 11; e.g., sample S11-8). The Hopkinson peak on the heating curve is sometimes very large, perhaps indicating the presence of two distinct magnetic phases.

Group III does not display a Hopkinson effect on the cooling curve. The mineral responsible for the Hopkinson effect on the heating curve therefore completely disappears during heating to 700 °C (Figure 11; e.g., sample S11-9). This is interpreted as the expression of inversion of titanomaghemite to other minerals. The T_c for Group I is therefore related to titanomagnetite and for Group III to titanomaghemite. The samples that correspond to Group II display a mixture of these two magnetic phases. It is therefore not possible to determine which mineral is chiefly responsible for the measured Curie temperature.

An exception is observed for sample S9-13. The thermomagnetic cycle of this sample displays a similar shape on the heating and cooling curves, although for different magnetic susceptibility amplitudes (Figure 11). The different amplitudes could be related to an atomic reorganization of the crystalline structure, which may increase magnetic susceptibility values during cooling without magnetic mineralogical transformations (Bina, 1990). The rapid decrease of k values that starts at $\approx$560 °C with an inflection at 572 °C, is in agreement with the Curie temperature of magnetite (O'Reilly, 1984). In both curves, a peak in magnetic susceptibility values is observed for temperatures near 280 °C. This thermomagnetic characteristic is consistent with the presence of titanomagnetite, as this characteristic is maintained after the

Table 1. Some magnetic properties of basalt samples. Group (see text); Tc – Curie temperature (°C); z – oxidation degree determined for a composition parameter of x=0.6 (Dunlop and Ozdemir, 1997); NRM_m – Natural Remanent Magnetization ($10^{-3}Am^2/kg$); NRM_v – Natural Remanent Magnetization (A/m); P-A, Pseudo-age (Ma).

Basalts	Lat. (°)	Long (°)	Group	Tc	Z	NRM_m	NRM_v	P-A
S6-1	N36.535	W33.446	II	261	0.16	3.7	10.1	0.6
S6-3	N36.547	W33.439	III	338	0.40	2.1	5.8	1.1
S6-4	N36.554	W33.434	III	255	0.15	0.9	2.4	0.5
S6-8	N36.562	W33.435	III	287	0.23	2.1	5.7	0.7
S7-12	N36.555	W33.433	II	318	0.33	4.1	10.9	0.9
S7-14	N36.559	W33.437	III	303	0.28	4.4	12.0	0.8
S9-10	N36.541	W33.423	III	235	0.11	2.5	6.9	0.5
S9-13	N36.550	W33.423		572		0.02	0.06	
S9-15	N36.551	W33.424	III	356	0.47	4.5	12.6	1.3
S9-16	N36.553	W33.427	II	258	0.16	1.4	3.9	0.6
S9-18	N36.556	W33.432	II	214	0.07	1.8	5.4	0.4
S10-9	N36.562	W33.435	II	330	0.37	1.8	4.3	1.0
S11-1	N36.564	W33.404	III	248	0.13	1.2	3.1	0.5
S11-2	N36.565	W33.410	II	184	0.02	2.6	6.6	0.4
S11-5	N36.564	W33.439	II	330	0.37	1.9	5.1	1.0
S11-8	N36.563	W33.441	II	196	0.04	3.4	9.0	0.4
S11-9	N36.564	W33.442	III	216	0.07	4.8	13.2	0.4
F11-1	N36.523	W33.448	I	170	≈0	1.9	4.9	≈0
F11-2	N36.583	W33.448	I	97	≈0	2.4	6.9	∼0
F11-3	N36.539	W33.45	II	229	0.09	3.1	7.4	0.5
F11-8	N36.540	W33.460	II	236	0.11	8.2	22.2	0.5
F11-10	N36.554	W33.451	I	215	0.07	1.4	3.8	0.4
F12-2	N36.563	W33.404	II	321	0.34	3.2	8.7	0.9
F12-15	N36.559	W33.435	III	309	0.30	2.6	7.1	0.8
F12-16	N36.562	W33.431	II	235	0.11	4.5	11.8	0.5
F13-2	N36.498	W33.419	I	174	≈0	2.1	5.7	≈0
F13-3	N36.498	W33.428	II	250	0.14	4.1	11.0	0.5
F13-5	N36.497	W33.433	III	291	0.24	3.1	8.5	0.7
F13-7	N36.493	W33.438	II	199	0.04	6.7	18.1	0.4

maximum temperature of 700 °C. Although two magnetic phases coexist, the magnetic phase of magnetite dominates the magnetic behavior because the variation related to titanomagnetite is weak when compared to the rapid decrease in magnetic susceptibility observed for temperatures higher than 560 °C.

Determination of oxidation degree

The low-temperature oxidation of titanomagnetite to titanomaghemite in oceanic basalts is one of the most important factors explaining the fall in NRM intensity (Irving, 1970; Marshall and Cox, 1972; Bleil and Petersen, 1983; Johnson and Pariso, 1993) and yielding information on the age of these basalts.

Microprobe techniques cannot be used to determine the chemical composition of titanomagnetites when the magnetic carriers are smaller than 5 μm (Grommé et al., 1979; Kent and Gee, 1996; Horen and Fleutelot, 1998). This problem is resolved by the use of electronic microscopy (Shau et al., 1993; Xu et al., 1997a,b; Zhou et al., 1997, 2000, 2001). Electronic microscopy permits the determination of the chemical composition of isolated titanomagnetite grains, which may not be representative of the sample total volume, given the possible variations of x between adjacent grains (Zhou et al., 1997). An alternative approach (Akimoto, 1962; Nishitani and Kono, 1983; Ozima and Larson, 1970; Schmidbauer and Readman, 1982; Uyeda, 1958) is based on the use of an empirical poly-

nomial fit of second order between x and T_c, given by

$$T_c = 575 - 552.7x - 213.3x^2, \quad (1)$$

which allows the determination of x as a function of T_c. Once this methodology is based on T_c, which is measured for the whole rock, we assume that x is representative of the rock volume.

This polynomial adjustment was made for the samples that belong to Group I, which include only titanomagnetite as magnetic carrier. The results provide values for x ranging between 0.54 and 0.68, with an average value near 0.6. These compositions are commonly found in oceanic basalts (e.g., Johnson and Hall, 1978; Peterson et al., 1979; Smith and Banerjee, 1986; Bina and Prévot, 1990), and are within the bounds proposed by Zhou et al. (2000) for the largest titanomagnetite grains in the interior of pillow lavas.

Curie temperatures for Groups II and III, which include titanomaghemites, are higher. We investigated if this difference is related to a variation in the x parameter or to another factor. In fact, TiO_2 content and the oxidation of titanomagnetites are important factors controlling the Curie temperature. With decreasing titanium content, the magnetic susceptibility values and Curie temperatures increase. In contrast, when the oxidation degree increases, the magnetic susceptibility values decrease but the Curie temperature increases (Day et al., 1977; Smith, 1987). In our samples, the decrease of susceptibility values correlates with a general increase of T_c (Figure 12). Variations of Curie temperatures are therefore mainly related to the variation of oxidation. We can assume that the original composition of titanomagnetites in all our samples is near $x = 0.6$.

The variation in the magnetic properties of samples from the Saldanha Massif is therefore mainly associated with maghemitization. To obtain a rough assessment of the oxidation state of titanomagnetites from basalts, the empirical relationship established by Ozdemir and O'Reilly (1982) and Brown and O'Reilly (1988) for $x = 0.6$ was used:

$$T_c = 170 + 630^*z - 657^*z^2 + 324^*z^3 \quad (2)$$

where z is the degree of oxidation. Although the maximum obtained value of z is 0.47, most of the samples display z-values lower than 0.3, corresponding to a low degree of oxidation for most of the basalts (see Table I).

Correlation between degree of oxidation and Natural Remanent Magnetization (NRM) intensity

NRM was measured with a Minispin Magnetometer (Molspin LTD). We found no clear correlation between the degree of oxidation and NRM intensity (Figure 13). One of the factors that influences NRM intensity is magnetic grain size. The NRM of SD ferromagnetic minerals displays the highest stability and intensity values (Day et al., 1977; Dunlop, 1981). In Figure 13, we show that SD samples ($Jrs/Js > 0.5$) correspond to the highest NRM intensities; therefore, magnetic grain size has a significant effect on intensity. Considering only samples with $Jrs/Js > 0.5$, there is a decrease in NRM intensity with increasing of z, and the relationship ($I^{NRM} = 5.78–7.30\ z$) can be obtained by linear regression. The variation in NRM intensity is thus mostly related to both grain size and oxidation degree.

Concerning the relation between NRM intensity and oxidation degree, our data display similar overall behavior, e.g., decrease in NRM intensity with low-temperature oxidation of titanomagnetites to titanomaghemites (Irving, 1970; Marshall and Cox, 1972; Bleil and Petersen, 1983; Johnson and Pariso, 1993). Recently, Zhou et al. (2001) based on electron microscopy and microprobe for the determination of z, show the same tendency, although our data are more clustered. This could be the result of the different methodologies utilized for the determination of the oxidation degree or to the relative mineralogical homogeneity of our samples. Although the methodologies utilized by Zhou et al. (2001) are very accurate, the value of z can vary considerably between adjacent grains, explaining the large scatter of their data. The methodology used to determine z for the samples from the Saldanha Massif could be representative of data from a much larger volume of rock.

Pseudo-ages

Zhou et al. (2001), based on electronic microscopic observations and magnetic properties of oceanic basalts, verified that z increases gradually with the age (t) of the samples, obtaining an empirical relation given by $z = p + q\ \log(t)$, with $p \approx 0.38$, $q \approx 0.38$, and t being the age in millions of years for $t > 0.1$ Ma. Considering this relationship, we can compute 'pseudo-ages' for Saldanha Massif basalts. The values obtained (Table I and Figure 15) show a max-

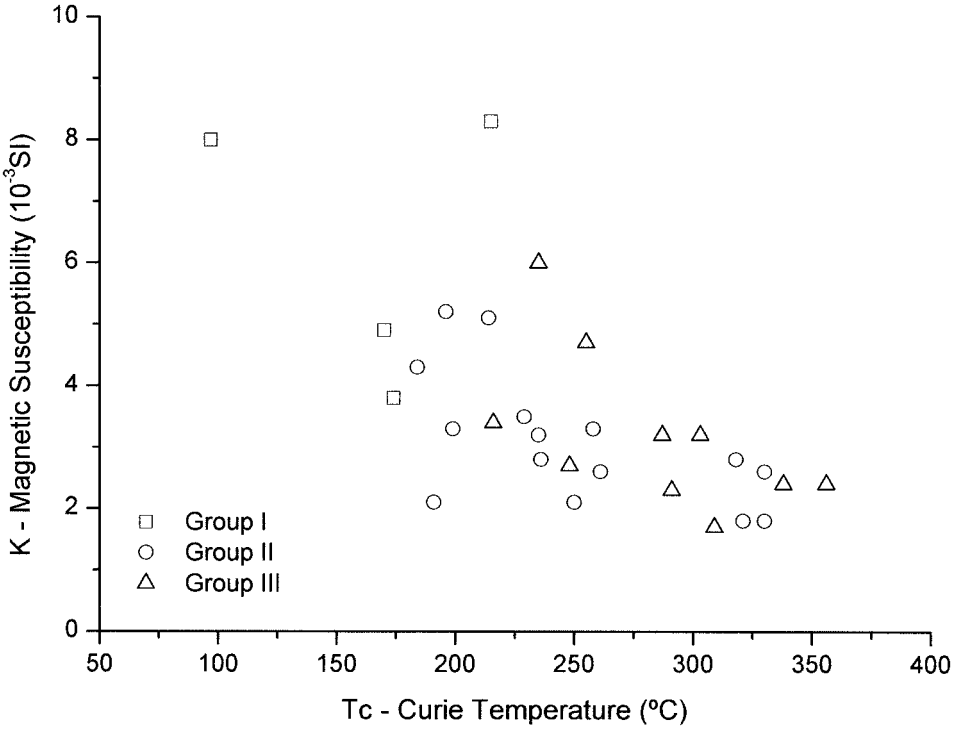

Figure 12. Curie temperature plotted *versus* magnetic susceptibility.

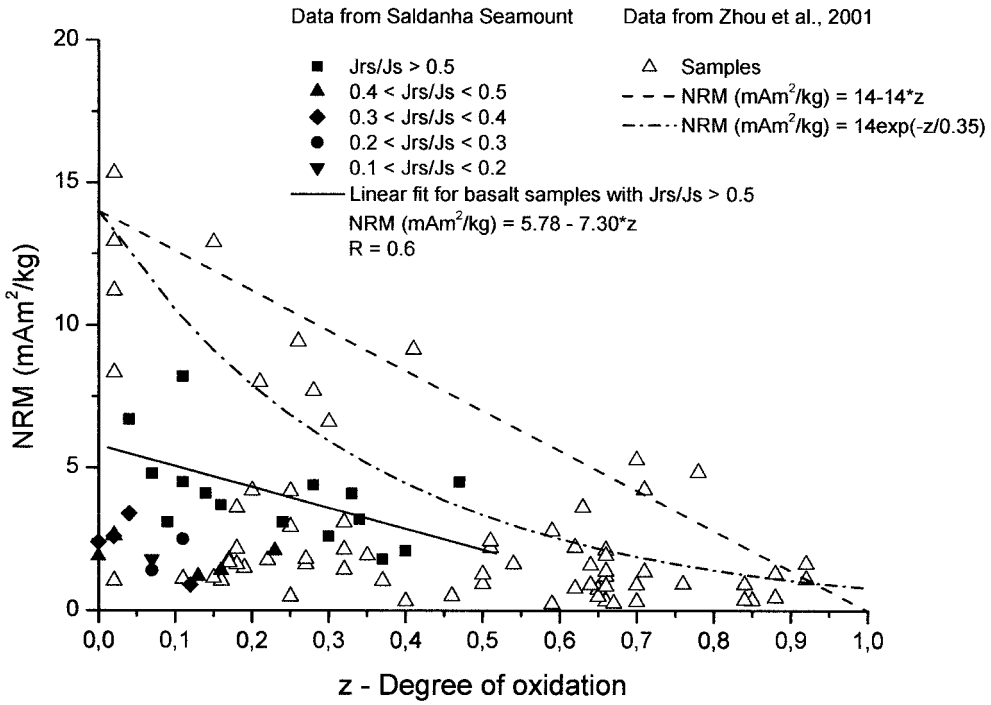

Figure 13. Degree of oxidation (z) *versus* Natural Remanent Magnetization (NRM) intensity.

imum age of 1.3 Ma, although most samples range between 0.4–0.6 Ma.

Discussion and Conclusions

Marine magnetic anomaly profiles constitute the main source of information on seafloor spreading kinematics. However, study of the magnetic properties of seafloor rocks gives us additional information on the mechanical and thermal processes that shaped the oceanic crust. Here, we discuss the magnetic fabric and the thermomagnetic properties of basalt samples from the Saldanha Massif and interpret them in a tectonic context deduced from bathymetry, sidescan sonar data and direct dive information.

Magnetic mineralogy

Titanomagnetite appears to be the original magnetic phase for the majority of basalt samples from the Saldanha Massif, with an average Ti^{4+} mole proportion of $x \approx 0.6$. Most basalt samples from the Massif also contain titanomaghemite, the result of low-temperature oxidation of titanomagnetite. Magnetic grains are predominantly single-domain, with high NRM values and lack of magnetic fabric, typical of rocks subjected to fast cooling, as is the case of pillow lavas.

The NRM variation inside our study area shows two distinct controlling factors for NRM intensity: grain size and oxidation state (see Figure 13). Magnetic carriers with single-domain grain size display higher NRM intensity values than samples with grain size between the limits of SD and PSD, indicating that SD carriers contribute significantly to the magnetic signature of the seafloor. Only minerals with $Jrs/Js > 0.5$ (i.e., for the SD grains, see Figures 9 and 13) show an inverse linear relationship between NRM intensity and oxidation degree.

Anomalous Sample S9-13

Basalt sample S9-13 is characterized by magnetite as the main magnetic carrier. It shows planar magnetic fabric, low NRM and high magnetic susceptibility values, as well as pseudo-single domain grain size. This pattern is interpreted as the result of high-temperature oxidation, also known as deuteric oxidation, which occurs when lava cools from 900 °C to 500 °C (Grommé et al., 1979; Tucker and O'Reilly, 1980). When the original magnetic phase corresponds to titanomagnetite with $x \approx 0.6$–0.7, the result of this oxidation process culminates in a low-Ti titanomagnetite, near the composition of magnetite, with high Curie temperature (Dunlop and Ozdemir, 1997). Smith and Banerjee (1986) analyzed basalt samples from DSDP/ODP Hole 504B in the upper kilometer of the Eastern Pacific Ocean, and found magnetite as the main magnetic carrier in the dyke complex. Shau et al. (1993), reanalyzing the samples from the same hole using STEM (Scanning Transmission Electron Microscopy) methods, concluded that the observed magnetite grains were primary, preserving typical structures of deuteric oxidation, and/or secondary, resulting from hydrothermal alteration. The low values of NRM, the high magnetic susceptibility and the pseudo-single domain size of the magnetite grains are in accordance with a significant contribution from multi-domain grains to the magnetic signature, suggesting slow cooling, typical of an intermediate crustal level.

Saldanha Massif emplacement mechanism

Serpentinized mantle rocks have been described in numerous tectonic contexts along the Mid-Atlantic Ridge [see Lagabrielle et al., (2000) and Karson et al., (2000) for a review]. Different emplacement mechanisms have been proposed involving vertical diapiric movements of serpentinitic mass (Bonatti, 1976), fault controlled uplift associated with serpentinization in depth (Francis et al., 1981) and more recently, implication of low angle normal faults that would act as the main driving mechanism for the exhumation process either as result of stages of amagmatic spreading (Karson and Dick, 1983; Tucholke and Lin, 1994) or else as result of asymmetries in the tectonic and magmatic processes governing extension at a spreading segment (Dick et al., 1981; Cannat,1993).

With regard to the Saldanha Massif emplacement mechanism, the lack of any clear evidence for the existence of any radial fracturation pattern seem to exclude the possibility of a diapiric type of emplacement. We believe instead that some sort of tectonic process probably involving detachment faulting has to be evoked to explain: (1) the distribution of the serpentinites from the base of the FAMOUS spreading axis to the AA depression, interpreted in this context as the fossil trace of a detachment fault nucleation zone; (2) the dome structure of the massif; (3) the general outcropping style, mainly composed of debris within the massif; (4) the existence of numerous ser-

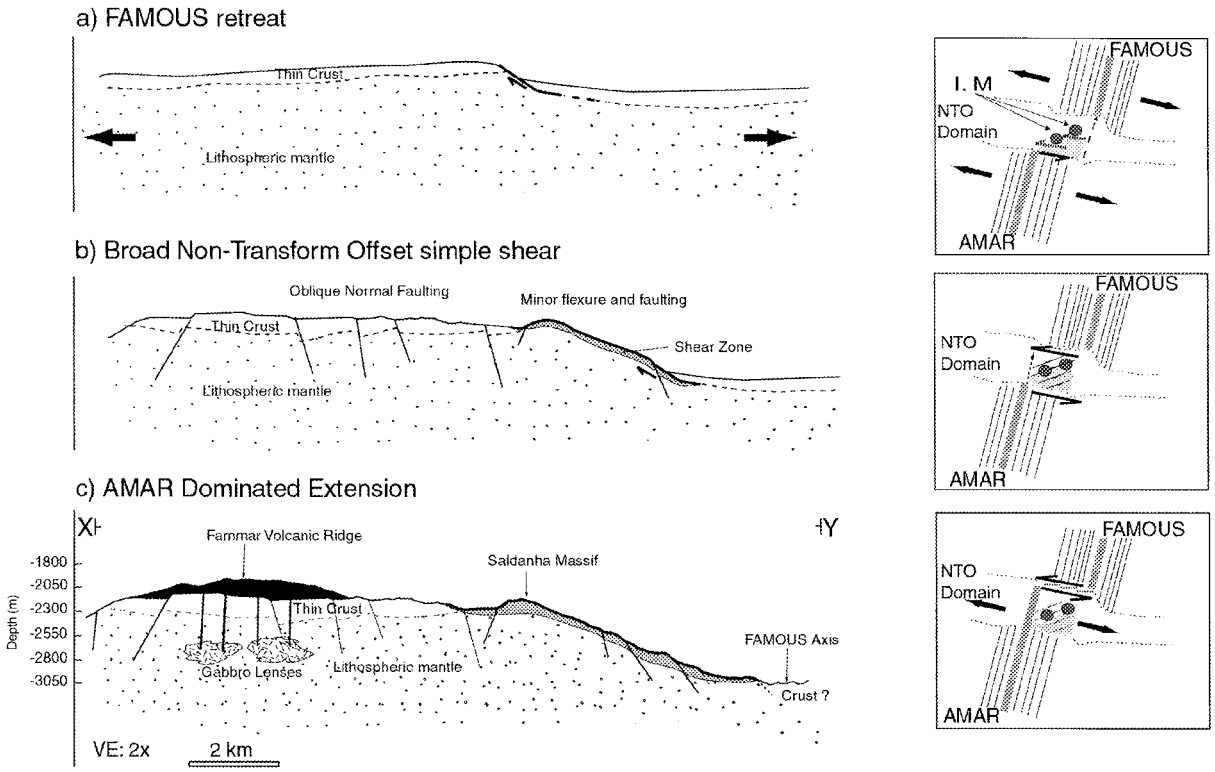

Figure 14. Interpretative cartoon displaying different evolutionary stages of the Saldanha Massif in cross section and plan view (boxes). (a) FAMOUS retreats and promotes development, probably by detachment faulting, of ephemeral intersection massifs (I.M.) which account for the FAMOUS valley western wall complex structure. Shaded light grey interpreted area represents incipient NTO bathymetric expression (WNW-ESE depressions south of the I.M.). Coeval tectonic up-lift leads to un-roofing of serpentinized mantle rocks exposed along the Saldanha Massif eastern flank. (b) Under lap between FAMOUS and AMAR segments could have resulted in a broad simple shear area with oblique NE-SW extension. Detachment activity probably ceased during this stage. Final stages of detachment fault might have result in minor lithosphere flexure as in detachments described in other oceanic areas. (c) FAMMAR progression towards north. AMAR Segment propagation results in migration of the NTO active zone northwards to its interpreted present position north of the FAMMAR ridge (cf. Goud and Karson, 1985) and allows for capturing of Saldanha Massif as AMAR off-axis lithosphere. See Figure 1 for topographic profile location. Geological model has no vertical scale. VE: vertical exaggeration of the topographical profile.

pentinitic ridges and small throw faults, as observed by submersible dives, with orientations ranging from E-W to WNW-ESE; and (5) the high heterogeneity of sampled lithotypes, not corresponding to a typical oceanic crust layout.

The majority of the above-mentioned characteristics could be accounted for by considering an emplacement mechanism similar to the oceanic core complexes described by Tucholke et al. (1998, 2001), Cann et al. (1997) and Blackman et al. (1998). However, these structures have a clear set of morphological characteristics (well-defined breakaway and terminator and sometimes strongly corrugated surfaces), which are not evident in the Saldanha massif. Moreover, these lineated massifs are generally associated with active or rafted Inside Corner Highs in generally stable Ridge-Transform Intersections (RTI), thus contrasting to the Saldanha Massif location within the FAMOUS-AMAR NTO. Gracia et al. (2000) suggested that the development of these isolated massifs within the NTO domains could be explained by mechanisms similar to inside corner high development provided that adjacent segments were in retreat during periods of amagmatic extension. The morphostructural variability, observed within the NTO, and the irregularity of the NTO off-axis trace seems to reflect a complex history of incursions and retreats of adjoining segments into and from the NTO domain. Such a process could account for the complex structure observed in the FAMOUS western wall and would imply that the different tectonic orientations within NTO are not contemporary and reflect the NTO evolution (see Figure 14 for detail).

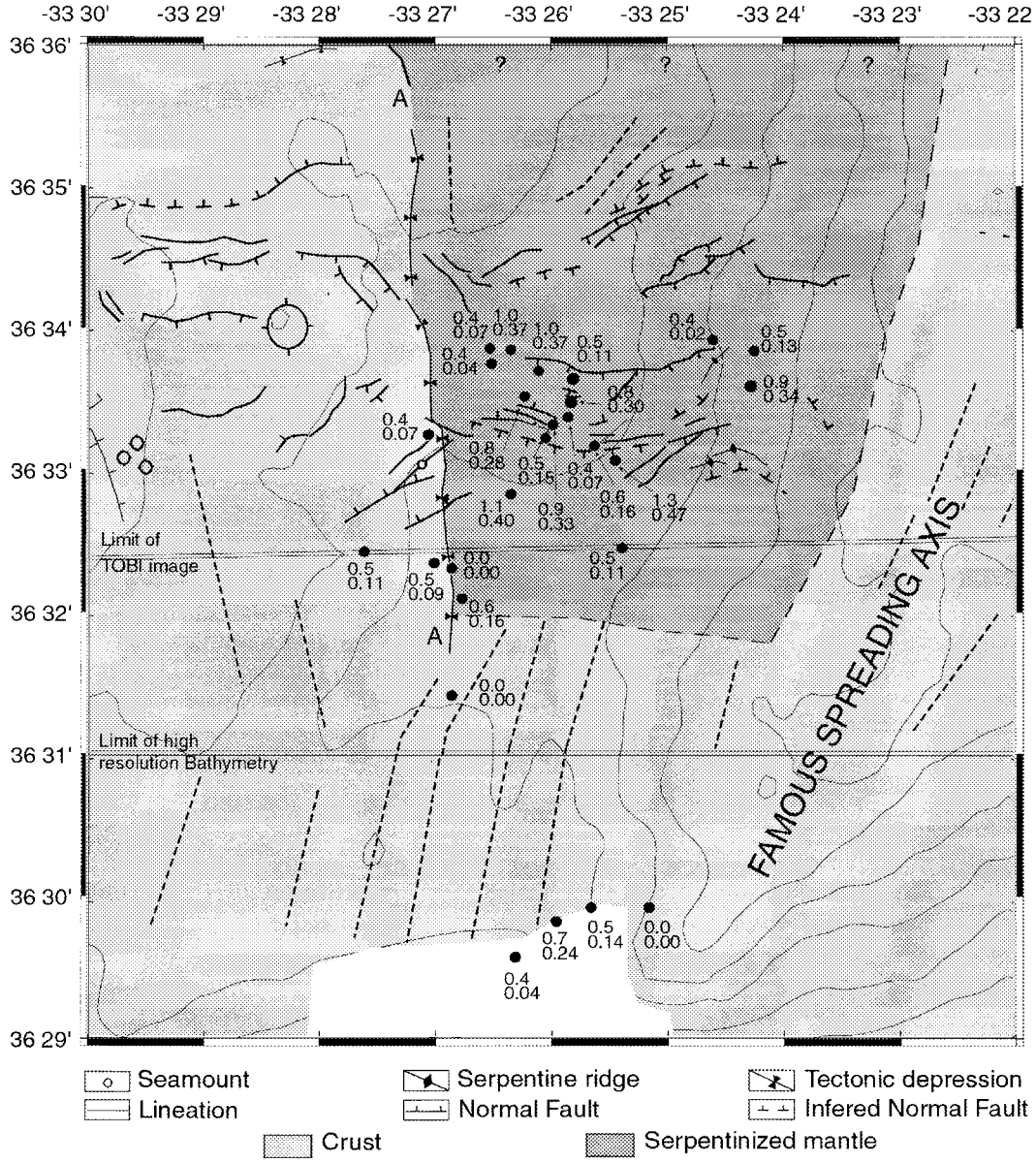

Figure 15. Spatial distribution of pseudo-ages (top values) and oxidation degree (bottom values) of the basalt samples in the Saldanha Massif. Cases where we can only deduce that samples are younger than 0.38 Ma are flagged as '0.0 Ma'. Thick black lines: structures mapped from TOBI images validated where possible from dives. Long dashed lines: interpreted limits of the Massif. Short dashed lines: lineations retrieved from bathymetry. Thin continuous lines are 200 m spaced bathymetric contours.

The relation of the Saldanha Massif with the neighboring FAMOUS segment displays a similar setting to the northern and southern intersection massifs of the OH3 segment, where serpentinized ultramafic occurrences were reported by Bideau et al. (1996). Similarly to the Saldanha Massif, these massifs as described by Lagabrielle et al. (2000) form rounded edifices that appear to be disconnected from the ridge flank walls and are separated from the region of ridge parallel fabric by an E-W depressed area. Diving in the massifs (Bideau et al., 1996; Gracia et al., 1997) revealed that the massif's surface is covered with sedimented talus of ultramafic rocks, thus reproducing the Saldanha massif observations. In the Southern massif a low angle fault surface with fine grain mylonites was identified (Lagabrielle et al., 2000).

The Saldanha Massif limits agree well with the spatial distribution of the measured oxidation degrees within and outside the Massif area (Figure 15). Almost all the samples belonging to Group III (higher oxidation degree) are located within the Massif, whereas samples from Group I (lower oxidation degree) are located outside it. The proposed tectonic mechanism can also support these observations. We believe that detachment fault surfaces can promote preferable pathways for fluid circulation in an essentially shallow environment thus explaining the higher low-temperature oxidation degrees of the Massif samples. On the contrary, samples from dive F13 approximately follow the expected increase in the oxidation degree with distance from the FAMOUS spreading axis.

The magnetic signature of sample S9-13, interpreted as originating from a mid-crustal level, does not fit the current sample position in the massif surface, associated with a rubble of basaltic breccias and confined within two major serpentinitic units. Such a setting suggests an allocthonous origin for this sample. We speculate that this sample and related basaltic breccias were probably part of a volcanic feeder of an overlaying extrusive layer, possibly within the FAMOUS valley. Triggering and continued displacement along the detachment fault could have resulted in subtraction of this unit from its original position and its passive emplacement to its present position as a remnant of the hanging wall.

Acknowledgements

This work is dedicated to Professor Luiz Saldanha, a leading Portuguese Marine Biologist, and scientific coordinator of AMAR research project, deceased in 1997.

We thank Dr Mathilde Cannat for SUDAZORES data, Dr Yves Fouquet for AMORES data and Dr Henri Bougault for MARFLUX data. Commentaries and suggestions made by reviewers greatly improved this manuscript. This work is part of AMAR – Research Project-PRAXIS/2/2.1/MAR/1748/95. Some of the present work was carried out in the framework of the bilateral cooperation ICCII:CNRS program.

References

Akimoto, S., 1962, Magnetic properties of Fe–Fe_2O_3 system as a basis of rock magnetism, *J. Phys. Soc. Jpn., suppl.* **B1** 707–710.

Alt, J. C., Honnorez, J., Laverne, C. and Emmermann, R., 1986, Hydrothermal alteration of a 1-km section valley of the upper oceanic crust, Deep Sea drilling Project Hole 504B: Mineralogy, chemistry, and evolution of seawater-basalt interactions, *J. Geophys. Res.* **91**, 10,309–10,335.

Barriga, F., Fouquet, Y., Almeida, A., Biscoito, M., Charlou, J. L., Costa, R., Dias, A., Marques, A., Miranda, J. M., Olu, K., Porteiro F., and Queiroz, M. G., 1999, Preliminary results of the Saldanha Cruise (FAMOUS segment of the MAR 36°30′ N), *Geophys. Res. Abstr.* **1**, Eur. Geophys. Soc., Den Haag.

Bideau, D., Hekinian, R., Bolinger, C., Constantin, M., Gracia, E., Guivel, G., Sichler, B., Apprioual, R. and Le Gall, R., 1996, Submersible investigation of highly contrasted magmatic activities recorded on two segments of the Mid-Atlantic Ridge near 34°52′ N and 33°55′ N, *Interridge News* **5**, 9–14.

Bina, M. M., 1990, Magnetic properties of basalts from ODP Hole 648B on the Mid-Atlantic Ridge near 23° N, *Proc. Ocean Drill Prog. Sci. Res.* **106/109**, 297–302.

Bina, M. M. and Prévot, M., 1989, Thermomagnetic investigations of titanomagnetite in submarine basalts: Evidence for differential maghemitization, *Phys. Earth Planet. Int.* **54**, 169–179.

Blackman, D. K., Cann, J. R., Janssen, B. and Smith, D. K., 1998, Origin of extensional core complexes: Evidences from the Mid-Atlantic Ridge, Atlantis Fracture Zone, *J. Geophys. Res.* **103**, 21315–21333.

Bleil, U. and Petersen, N., 1983, Variations in magnetization intensity and low-temperature titanomagnetite oxidation of ocean floor basalts, *Nature* **301**, 384–388.

Bougault, H., German, C., Miranda, J. M. and Marflux/ATJ. 1996, Mid-Atlantic Ridge: Hydrothermal fluxes at the Azores Triple Junction, *Interridge News* **5**(2), 13–17.

Bougault, H., Aballéa, M., Radford-Knoery, J., Charlou, J. L., Jean Baptiste, P., Appriou, P., Needham, H. D., German, C. and Miranda, J. M., 1998, FAMOUS and AMAR segments on the Mid-Atlantic Ridge: ubiquitous hydrothermal Mn, CH_4, δ^3He signals along the rift through walls and rift offsets, *Earth Planet. Sci. Lett.* **161**, 1–17.

Bonnati, E., 1976, Serpentinite intrusions in the oceanic crust, *Earth and Planet. Sci. Lett.* **32**, 107–113.

Brown, K. and O'Reilly, W., 1988, The effect of low-temperature oxidation on the remanence of TRM-carrying titanomagnetite $Fe_{2.4}Ti_{0.6}O_4$, *Phys. Earth Planet. Int.* **52**, 108–116.

Cann, J. R., Blackman, D. K., Smith, D. K., McAllister, E., Janssen,B., Mello, S., Avegerinos, E., Pascoe, A. R. and Escartin, J., 1997, Corrugated slip surfaces formed at North Atlantic Ridge – transform intersections, *Nature* **385**, 329–332.

Cannat, M., 1993, Emplacement of mantle rocks in the seafloor at the Mid-Atlantic ridge, *J. Geophys. Res.* **98**, 4163–4172.

Cannat, M., Briais, A., Deplus, C., Escartín, J., Georgen, J., Lin, J., Mercouriev, S., Meyzen, C., Muller, M., Pouliquen, G., Rabain, A. and Silva, P. 1999, 'Mid-Atlantic Ridge-Azores hotspot interactions: along-axis migration of a hotspot-derived event of enhanced magmatism 10 to 40 Ma ago', *Earth Planet. Sci. Lett.* **173**, 257–269.

Canon-Tapia E., Walker G. P. L. and Herrero-Bervera E., 1995, Magnetic fabric and flow direction in basaltic Pahoehoe lava of Xitle Volcano, Mexico, *J. Volcanol. Geotherm. Res.* **65**, 249–263.

Charlou J. L., Bougault, H., Donval, J. P., Pellé, H., Langmuir C. H. and C. F. S. Team. 1993, Seawater CH_4 concentration over the Mid-Atlantic Ridge, from Hayes F. Z. to the Azores Triple Junction, *EOS* **74**, 380.

Chevallier, R. and Pierre, J., 1932, Propriétés magnétiques des roches volcaniques, *Ann. Phys.* **18**, 383–477.

Day, R., Fuller, M. and Schmidt, V. A., 1977, Hysteresis properties of titanomagnetites: Grain size and compositional dependence, *Phys. Earth Planet. Inters.* **13**, 260–267.

DeMets, C., Gordon, R. G., Argus, D. F. and Stein, S., 1994, Effects of recent revisions to the geomagnetic reversal time scale on estimates of current plate motions, *Geoph. Res. Lett.* **21**, 2191–2194.

Dick, H. J. B., Thompson, G. and Bryan, W. B., 1981, Low-angle faulting and steady-state emplacement of plutonic rocks at ridge transform intersections, *Am. Geophys. Union Trans. EOS* **62**, 406.

Dunlop, D. J., 1981, The rock magnetism of fine particles, *Phys. Earth Planet. Inter.* **26**, 1–26.

Dunlop, D. J., 1986a, Hysteresis properties of magnetite and their dependence on particle size: A test of pseudo-single-domain remanence models, *J. Geophys. Res.* **91**, 9569–9584.

Dunlop, D. J., 1986b, Coercive force and coercivity spectra for submicron magnetites, *Earth Planet. Sci. Lett.* **78**, 288–295.

Dunlop, D. J. and Ozdemir, O., 1997, Rock Magnetism: Fundamentals and frontiers, *Cambridge University Press*, 573 pp.

Fouquet, Y. and Scientific Party, 1997, Cruise report, FLORES cruise, AMORES project of the European MAST III programme Plouzané, IFREMER, DRO/GM.

Francis, T. J. G., 1981, Serpentinization faults and their role in the tectonics of slow-spreading ridges, *J. Geophys. Res.* **86**, 11616–11622.

Gallagher, K. J., Feitknecht, W. and Mannweiler, U., 1968, Mechanism of oxidation of magnetite to γ-Fe_2O_3, *Nature* **217**, 1118–1121.

German C. R., Parson, L. M. and the HEAT Scientific Team, 1996, Hydrothermal exploration at the Azores Triple Junction: Tectonic control of venting at slow spreading ridges? *Earth. Planet. Sci. Lett.* **138**, 93–104.

German C., Richards K., Rudnicki M. D., Lam M. M., Charlou J. L. and the FLAME Scientific Party, 1998, Topographic control of a dispersing hydrothermal plume, *Earth Planet. Sci. Lett.* **156**, 267–273.

Gracia, E., Charlou, J. L., Radford-Knoery, J. and Parson, L., 2000, Non-transform offsets along the Mid-Atlantic Ridge south of the Azores (38°–34° N): Ultramafic exposures and hosting of hydrothermal vents, *Earth Planet. Sci. Lett.* **177**, 89–103.

Gracia, E., Bideau, D., Hekinian, R., Lagabrielle, Y., Parson, L. M., 1997, Along-axis magmatic oscillations and exposures of ultramafic rocks in a second-order segment of the Mid-Atlantic Ridge (33°43′ N to 34°07′ N), *Geology* **25**(12), 1059–1062.

Goud, M. R., Karson, J. A., 1985, Tectonics of short-offset. Slow slipping transform zones in the FAMOUS area, Mid-Atlantic Ridge, *Marine Geophys. Res.* **7**, 489–514.

Grommé, C. S., Wright, T. L. and Peck, D. L., 1979, Magnetic properties and oxidation of iron-titanium oxide minerals in Alae and Makaopuhi lava lakes, Hawaii, *J. Geophys. Res.* **74**, 5277–5293.

Honnorez, J., Honnorez-Guerstein, B. M., Worm, H.-U. and Laverne, C., 1996, Correlation among the changes with alteration in mineralogical, chemical, and magnetic properties of upper ocean crust, Hole 896A, *Proc. Ocean Drill. Prog. Sci. Res.* **148**, 171–190.

Horen, H. and Fleutelot, C., 1998, Highly magnetised and differentiated basalts at 18°–19° S propagating spreading centre in the North Fiji Basin, *Mar. Geophys. Res.* **20**, 129–137.

Irving, E., 1970, The Mid-Atlantic Ridge at 45° N, XVI. Oxidation and magnetic properties of basalts; review and discussion, *Can. J. Earth Sci.* **7**, 1528–1538.

Jelinek V., 1977, The statistical theory of measuring anisotropy of magnetic susceptibility of rocks and its application, *Brno, Geofyzika*, 1–88.

Jelinek V., 1981, Characterization of the magnetic fabric of rocks, *Tectonophysics* **79**, 63–67.

Johnson, H. P. and Hall, J. M., 1978, A detailed rock magnetic and opaque mineralogy study of the basalts from the Nazca plate, *Geophys. J. R. Astr. Soc.* **52**, 45–64.

Johnson, H. P. and Pariso, J. E., 1993, Variations in oceanic crustal magnetization: Systematic changes in the last 160 million years, *J. Geophys. Res.* **98**, 435–445.

Karson, J. A., 2000, Internal structure of oceanic lithosphere: A perspective from tectonic windows. In: Faulting and magmatism at Mid-Ocean Ridges. *AGU Geophysical Monograph* **106**, 177–218.

Karson, J. A. and Dick, H. J. B., 1983, Tectonics of ridge-transform intersections at the Kane fracture zone, *Mar. Geophys. Res.* **6**, 51–98.

Kent, D. V. and Gee, J., 1996, Magnetic alteration of zero-age oceanic basalt, *Geology* **24**(8), 703–706.

Klinkhammer, G. P., Chin, C. S. and Wilson, C. 1992, Surveys of FARA section of the Mid-Atlantic Ridge for hydrothermal activity during FAZAR, *EOS* **74**(16), 380.

Lagabrielle, Y., Bideau, D., Cannat, M., Karson, J.A. and Mével, C. 2000, Ultra-mafic plutonic rock suites exposed along the Mid-Atlantic Ridge (10° N–30° N). Symmetrical-assymetrical distribution and implications for the seafloor spreading processes. In: Faulting and magmatism at Mid-Ocean Ridges. *AGU Geophys. Monogr.* **106**, 153–173.

Langmuir, C. H., Fornari, D., Colodner, D., Chalou, J. L., Costa, I., Desbruyères, D., Desonie, D., Emerson, T., Fiala-Medoni, A., Fouquet, Y., Humphris, S., Saldanha, L., Sours-Page, R., Thatcher, M., Tivey, M., Van Dover, C., Von Damm, K., Wiess, K. and Wilson, C., 1993, Geological setting and characteristics of the Lucky Strike vent field at 37°17′ N on the MAR, *EOS* **74**, 99.

Marshal, M. and Cox, A., 1972, Magnetic changes in pillow basalt due to sea floor weathering, *J. Geophys. Res.* **77**, 6459–6469.

Needham, H. D., Voisset, M., Renard, V. and Bougault, H., 1992, Structural and Volcanic Features of the Mid-Atlantic Rift Zone Between 40° N and 33° N, *EOS, Trans. AGU*, Fall Meeting **552** (Abstract).

Nishitani, T. and Kono, M., 1983, Curie temperature and lattice constant of oxidized titanomagnetite, *Geophys. J. R. Astr. Soc.* **74**, 585–600.

O'Reilly, W., 1984, Rock and Mineral Magnetism. Blackie, Glasgow and London & Chapman and Hall, New York, 220 pp.

Ozdemir, O. and O'Reilly, W., 1982, An experimental study of thermoremanent magnetization acquired by synthetic monodomain titanomaghemites, *J. Geomag. Geoelec.* **34**, 467–478.

Ozdemir, O., 1987, Inversion of titanomaghemites, *Phys. Earth Planet. Inter.* **46**, 184–196.

Ozima, M. and Larson, E. E., 1970, Low- and high-temperature oxidation of titanomagentite in relation to irreversible changes in the magnetic properties of submarine basalts, *J. Geophys. Res.* **75**, 1003–1018.

Parson, L., Grácia, E., Coller, D., German, C. and Needham, D., 2000, Second-order segmentation: the relationship between volcanism and tectonism at the MAR, 38° N–35°40′ N, *Earth Planet. Sci. Lett.* **178**, 231–251.

Peterson, N., Eisenach, P. and Bleil, U., 1979, Low temperature alteration of the magnetic minerals in ocean floor basalts. Talwani, M., Harrison, C. G. A. and Hayes, D. E. (eds.) Deep Drilling Res-

ults in the Atlantic Ocean: Ocean Crust, Maurice Ewing Series., pp. 169–209, AGU, Washington, D.C., Vol. 2.

Readman, P. W. and O'Reilly, W., 1972, Magnetic properties of oxidized (cation-deficient) titanomagnetites, (Fe, Ti,□)O_4, *J. Geomag. Geoelec.* **24**, 69–90.

Shau, Y. H., Peacor, D. R. and Essene, E. J., 1993, Formation of Magnetic Single-Domain magnetite in Ocean Ridge basalts with implications for sea-floor magnetism, *Science* **261**, 343–345.

Schmidbauer, E. and Readman, P. W., 1982, Low temperature magnetic properties of Ti-rich Fe-Ti spinels, *J. Magn. Magn. Mater.* **27**, 114–118.

Smith, G. M. and Banerjee, S. K., 1986, Magnetic structure of the upper kilometer of the marine crust at Deep Sea Drilling Project Hole 504B, Eastern Pacific Ocean, *J. Geophys. Res.* **91**(B10), 10337–10354.

Smith, B. M., 1987, Consequences of the maghemitization on the magnetic properties of submarine basalts: Synthesis of previous works and results concerning basement rocks from mainly DSDP legs 51 and 52, *Phys. Earth Planet. Inter.* **46**, 206–226.

Smith-Daignières, B., 1984, Propriétés magnétiques de roches basaltiques provenant de la couche 2 de la croûte océanique. Effets du degré de cristallisation et de l'altération a basse temperature. *PhD thesis*, University of Paris VI, France.

Tucker, P. and O'Reilly, W., 1980, The laboratory simulation of deuteric oxidation of titanomagnetites: Effect on magnetic properties and stability of thermoremanence, *Phys. Earth Planet. Inter.* **23**, 112–133.

Tucholke, B. E., Lin, J. and Kleinrock, M. C., 1998, Megamullions and mullion structure defining oceanic metamorphic core complexes on the Mid-Atlantic Ridge, *J. Geophys. Res.* **103**, 9857–9866.

Tucholke, B. E., Fujioka, K., Ishihara, T., Hirth, G. and Kinoshita, M., 2001, Submersible study of an oceanic megamullion in the Central North Atlantic, *J. Geophys. Res.* **106**, 16145–16161.

Uyeda, S., 1958, Thermo-remanent magmetism as a medium of paleomagnetism, with special reference to reverse thermo-remanent magnetism, *Jpn. J. Geophys.* **2**, 1–23.

Xu, W., Peacor, D. R., Dollase, W. A., Van Der Voo, R. and Beaubouf, R., 1997a, Transformation of titanomagnetite to titanomaghemite: A slow, two-step, oxidation-ordering process in MORB, *Am. Miner.* **82**, 1101–1110.

Xu, W., Van Der Voo, R., Peacor, D. R. and Beaubouf, R., 1997b, Alteration of fine-grained magnetite and its effects on the magnetization of the ocean floor, *Earth Planet. Sci. Lett.* **151**, 279–288.

Zhou, W., Van Der Voo, R. and Peacor, D. R., 1997, Single-domain and superparamagnetic titanomagnetite with variable Ti content in young ocean-floor basalts: No evidence for rapid alteration, *Earth Planet. Sci. Lett.* **150**, 353–362.

Zhou, W., Peacor, D. R., Van Der Voo, R. and Mansfield, J., 1999, Determination of lattice parameter, oxidation state, and composition of individual titanomagnetite/titanomaghemite grains by TEM, *J. Geophys. Res.* **104**, 17689–17702.

Zhou, W., Van Der Voo, R., Peacor, D. R. and Zhang, Y., 2000, Variable Ti-content and grain size of titanomagnetite as a function of cooling rate in very young MORB, *Earth Planet. Sci. Lett.* **179**, 9–20.

Zhou, W., Van Der Voo, R., Peacor, D. R., Wang, D. and Zhang, Y., 2001, Low-temperature oxidation in MORB of titanomagnetite to titanomaghemite: A gradual process with implications for marine magnetic anomaly amplitudes, *J. Geophys. Res.* **106**(B4), 6409–6421.